CONTRACT NAS 7-489

Stress Corrosion Cracking of Titanium Alloys

Heat Treatment Effects, SCC Velocity in Various Solvents and Electrochemical Kinetics with Ti:8-1-1 Alloy

Quarterly Progress Report No. 2

for Period of

October 1, 1966 through December 31, 1966

Prepared by

T. R. Beck

Solid State Physics Laboratory

Boeing Scientific Research Laboratories

Seattle, Washington 98124

N67-28006

1.0 Summary

2.0 Introduction

3.0 Technical Discussion

3.1 SCC Under Potentiostatic Conditions

3.2 Effect of Heat Treatment

3.3 SCC Under Open Circuit Conditions

3.4 Kinetics of Oxidation

3.5 Theory

4.0 Conclusions

5.0 Future Work

6.0 References

7.0 Appendix

Extended Abstract, "Analysis of Current Density Distribution in a Propagating Stress Corrosion Crack".

1.0 SUMMARY

Stress corrosion cracking of titanium:8%Al-1%Mo-1%V alloy was studied using techniques previously developed at Boeing. Precracked specimens were introduced to the studies resulting in lower failure loads and providing a wider range of stress for study. Heat treatment effects and various solvent environments were investigated. Electrochemical kinetic measurements were made to obtain more quantitative numbers for the parameters used in the electrochemical models describing velocity control.

One of the interesting findings is that SCC of Ti:8-1-1 occurred in pure water and methanol, but could be suppressed by addition of small amounts of nitrate or sulfate - on the order of 10-100 ppm. Ti:8-1-1 was also susceptible to SCC in chlorinated solvents such as carbon tetrachloride, methylene chloride and trichlorethylene. Heat treatment has a very marked effect on fracture load and crack velocity. Evidence from the kinetic studies indicates that the hydride mechanism does not play a role in SCC of Ti:8-1-1 under the conditions used in this work.

2.0 INTRODUCTION

This report describes part of a study of stress corrosion cracking of titanium alloys initiated in July 1965 (Ref. 1), and continued under NASA sponsorship beginning July 1966. The first Quarterly report on this contract covered the period from July 1 through September 30, 1966 (Ref. 2). The present report covers the period October 1 through December 31, 1966. In this period close cooperation continued with Dr. N. M. Lowry who is supported by a ARPA "coupling" program and with Dr. M. J. Blackburn of Boeing Scientific Research Laboratories who is in part supported by the present NASA contract. Dr. Blackburn contributed the section on effect of heat treatment.

3.0 TECHNICAL DISCUSSION

3.1 SCC Under Potentiostatic Conditions

A technique for precracking the notched tensile specimens was worked out and applied. The fatigue cracks were made by flexing specimens at the midsection with four-point loading. The dimensions of the flexing device are shown in Fig. 1. The peak to peak deflection of the machine was about 0.8 cm ($\frac{20}{64}$ inch). 400 cycles (at 1725 cycles per minute) was sufficient to cause small quarter-circle fatigue crack zones on each side of a 0.001 root radius machined notch in a 0.060 inch thick specimen as also shown in Fig. 1. The radii of the fatigue crack zones measured from the corners of the root of a notch were nearly one-half the sheet thickness.

Results with precracked and non-precracked specimens are compared in Fig. 2. The load at which square fracture initiated was significantly reduced at potentials of susceptibility in 0.6 M KCl solution. The crosshead was stopped when square fracture initiated so this is also the maximum load. This procedure produced a longer square fracture than that produced by allowing continued crosshead movement. Specimens with cracks preinitiated at -500 mv (Ref. 2) appeared to fail at loads between those of the precracked and the non-precracked specimens.

Further comparisons of ultimate load for precracked and non-

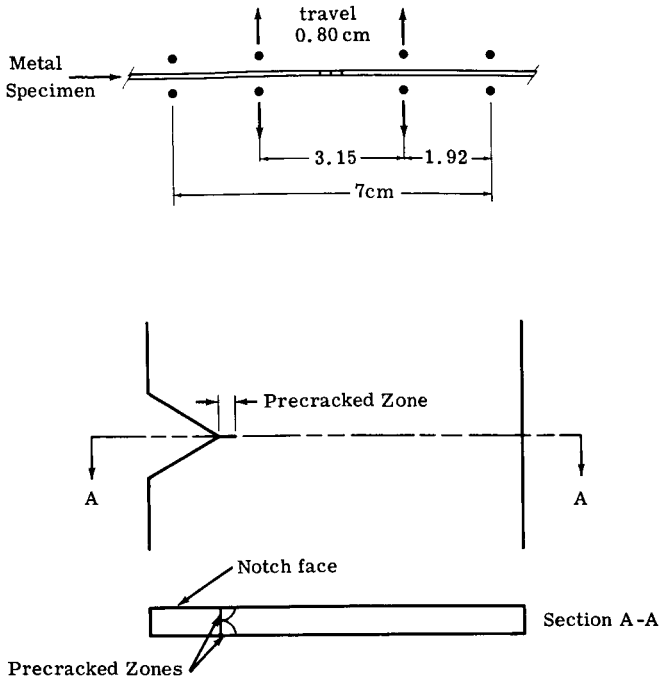

Fig. 1 Dimensions of Flexing Device and Appearance of Fatigue Crack.

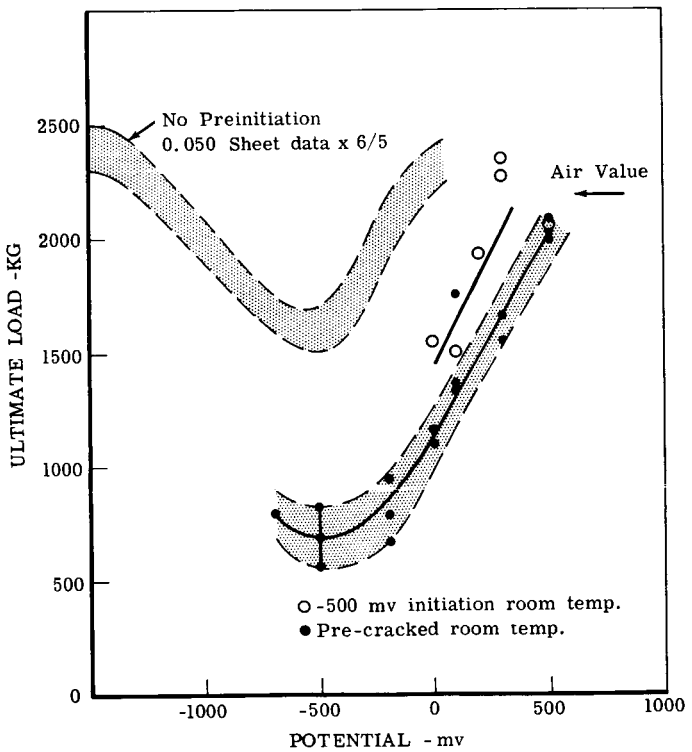

Fig. 2 Ultimate Load of 0.060 in. Duplex Annealed Ti:8-1-1 in 0.6 M KCl, Effect of Preinitiation and Precracking.

precracked specimens are shown in Table 1. The air valve for precracked specimens was slightly reduced from the non-precracked level, probably due to the reduced net cross sectional area. The significant decrease in ultimate load for precracked specimens at -500 mv in 0.6 M chloride solutions is seen. Interestingly, reinitiation of SCC in precracked specimens after stopping the crack occurred at a slightly higher load than the initiation. Reinitiation of a crack preinitiated electrochemically at -500 mv occurred at a slightly lower load than the preinitiation.

Corresponding data for mill annealed Ti:8-1-1 are given in Table 2. Results in air are similar to those for duplex annealed Ti:8-1-1. Whereas notched mill annealed Ti:8-1-1 specimens did not show loss of strength from air valves in 0.6 M chlorides at -500 mv, precracking caused a further loss of strength.

Two additional anions, cyanide and thiocyanate were tested in a few runs with no apparent susceptibility as noted in Table 3. To date, chloride, bromide and iodide are the only anions found to produce SCC in aqueous solution under potentiostatic conditions.

PRECRACKED SPECIMENS

Run No.	Environment	Ultimate load - kg		
		initiation	reinitiation	
L257	Air	2310		
L258	Air	2240		
		2275		Avg.
674	0.6 M KCl -500 mv	490	532	
675		560	605	
676		508	516	
677		700	686	
678		620	740	
679		644	800	
680		634	692	
681		618	630	
683		648	686	
684		674	706	
685		436	702	
		595	662	Avg.

Table 1. Comparison of Ultimate Load of Precracked and Non-Precracked Duplex Annealed Ti:8-1-1 (Sheet No. 2194, (Ref. 1), Thickness 0.060 in., Crosshead Speed 0.005 cm/min, Room Temp.)

(NON-PRECRACKED) NOTCHED SPECIMENS

Run No.	Environment	Ultimate load - kg	
526	Air	2600	
527	↓	2445	
528		2495	
529		2605	
		2540	Avg.
530	0.6 M NaCl -500 mv	1460	
531	↓	1795	
532		1350	
533		1570	
534		1700	
535		1345	
		1530	Avg.

Run No.	Environment	initiation	reinitiation	
576	0.6 M KCl -500 mv	1500	1500	
577	↓	1690	1555	
578		1690	1585	
579		1655	1605	
580		1645	1100	
581		1840	1570	
582		1770	1225	
583		1640	1100	
584		2000	1850	
585	0.6 M KCl -500 mv	1805	1600	
586	↓	1970	1690	
588		1705	1555	
589		1950	1595	
665	0.6 M KCl -500 mv	1500	1235	
666	↓	1400	1225	
667		1750	1705	
668		1640	1495	
669		2025	1900	
		1730	1510	Avg.

Run No.	Environment	Ultimate load - kg	
Precracked			
699	Air	1110	
700	Air	1200	
		1155	Avg.
701	0.6 M KCl -500 mv	440	
702	0.6 M KCl -500 mv	548	
		495	Avg.
Non-Precracked			
72	Air	1310	
73	Air	1260	
		1285	Avg.
75	0.6 M LiCl -500 mv	1270	
77	0.6 M LiCl -500 mv	1340	
79	0.6 M LiCl -500 mv	1400	
		1340	Avg.

Table 2. Comparison of Ultimate Load of Precracked and Non-Precracked Mill Annealed Ti:8-1-1 (Sheet No. 2026, (Ref. 1), Thickness 0.060 in., Crosshead Speed 0.005 cm/min, Room Temp.)

Run No.	Environment	Ultimate load - kg
716	0.6M NaCNS -500 mv	2150
717	0.6M NaCNS 0 mv	2285
718	0.6M NaCNS +500 mv	2055
719	0.6M NaCNS +1000 mv	2100
720	0.6M KCN -500 mv	1926
721	0.6M KCN 0	2135
722	0.6M KCN +500 mv	2235

Table 3. Ultimate Load of Precracked Duplex Annealed Ti:8-1-1 in Cyanide and Thiocyanate (Sheet No. 2194, (Ref. 1) Thickness 0.060 in., Crosshead Speed 0.005 cm/min, Room Temp.)

3.2 Effect of Heat Treatment

The variation of fracture stress with heat treatment for the alloy Ti:8Al:1Mo:1V in air and 0.6 M KCl is shown in Fig. 3. Specimens were solution treated in temperatures between 500°C and 1100°C and subsequently water quenched. Testing was conducted on fatigue cracked specimens. Testing in the 0.6 M KCl solution was performed at -500 mv as this has been shown to be in the range of maximum susceptibility to SCC. It can be seen from Fig. 3 that the fracture strength increases with solution treatment temperature in both air and 0.6 M KCl, the increase in strength in KCl being most rapid between 900 and 1000°C. The phase structure of this alloy has been investigated in some detail (Ref. 3,4) and the variation of structure with quenching temperature is indicated in Fig. 3. The decrease fracture stress in air is associated with increasing tendency to form short range order (SRO) and eventually particles of the phase α_2 (based on Ti_3Al). This essentially precipitation hardening reaction has been shown to increase the yield strength and decrease the ductility and notch strength. It is apparent that this transformation does not produce a great change in the initiation stress in KCl, but there is evidence that it can change the crack propagation velocity. It is tempting to associate the large change in fracture strength in KCl between 900°C - 1000°C to the martensitic transformations that occur in the β-phases on quenching. It is considered, however, that a more important change is in the relative volume fraction of the α and β-phases present at these temperatures. This

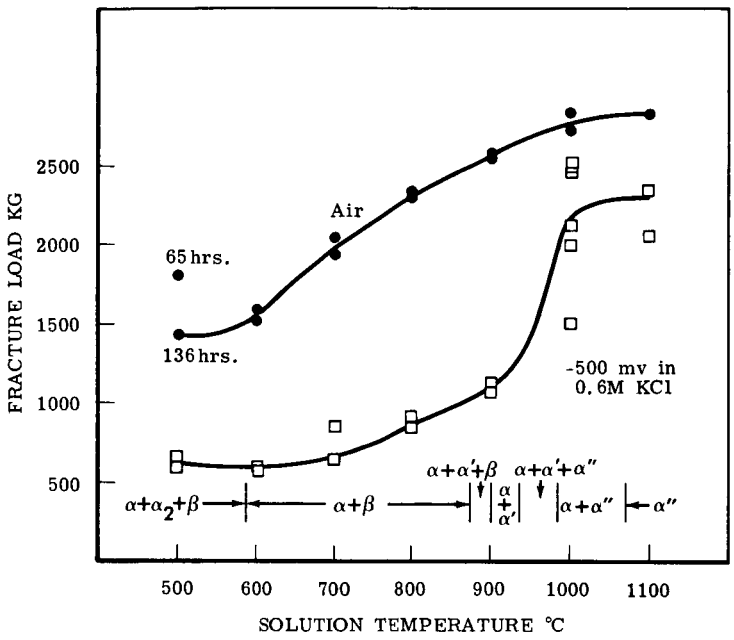

Fig. 3 Variation of Fracture Load with Solution Temperature for Ti:8Al-1Mo-1V.

change is illustrated in the optical micrographs in Fig. 4. Fractography results have shown that failure under SCC condition occurs by apparent cleavage in the α-phase and ductile failure of the β-phase. From this observation it is concluded that the α-phase controls susceptibility to SCC, and factors which influence brittle failure of the α-phase will likewise influence susceptibility to SCC. In this case we can list at least three such factors.

(1) Grain size and probably more important in α + β alloys, mean free path in the α-phase. It can be seen from Fig. 4 that although there is a slight increase in grain size at 1000°C, there is a decrease in mean free path within the α-phase.

(2) Composition: Any reduction in aluminum content of the α-phase will reduce susceptibility. With increasing solution treatment temperature dilution of the α-phase by vanadium and molybdenum occurs.

(3) Possibly a reduction in the degree of SRO in the α-phase. The ability of the α-phase to relax stress concentrations is related to the ability of dislocations to cross slip which will be related to the degree of SRO. Increasing solution treatment temperatures would be expected to reduce SRO.

Work is being performed on binary titanium aluminum alloys to investigate more quantitatively the above effects. Investigations of the variation crack propagation velocity, with heat treatment in Ti:8-1-1, is also in progress.

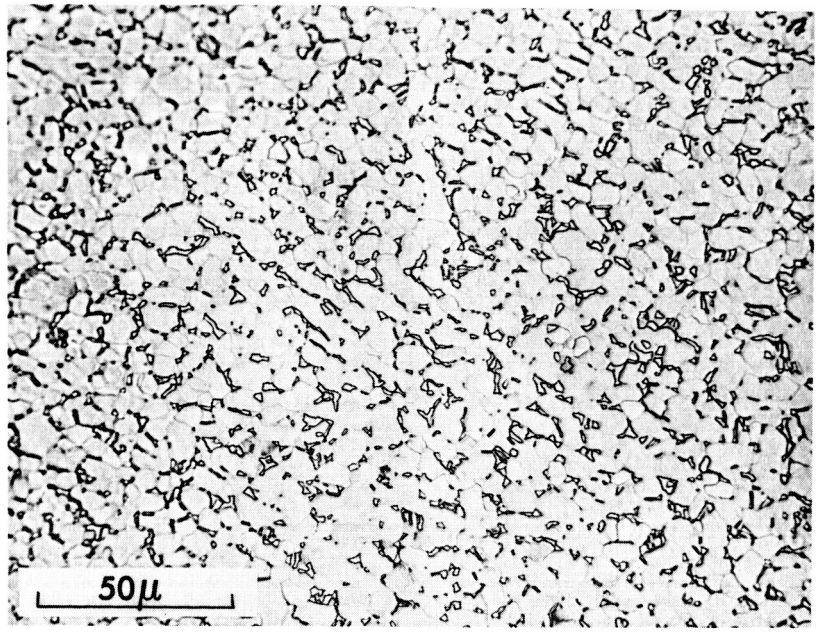

965 500x

Ti 8-1-1 quenched from 900°C

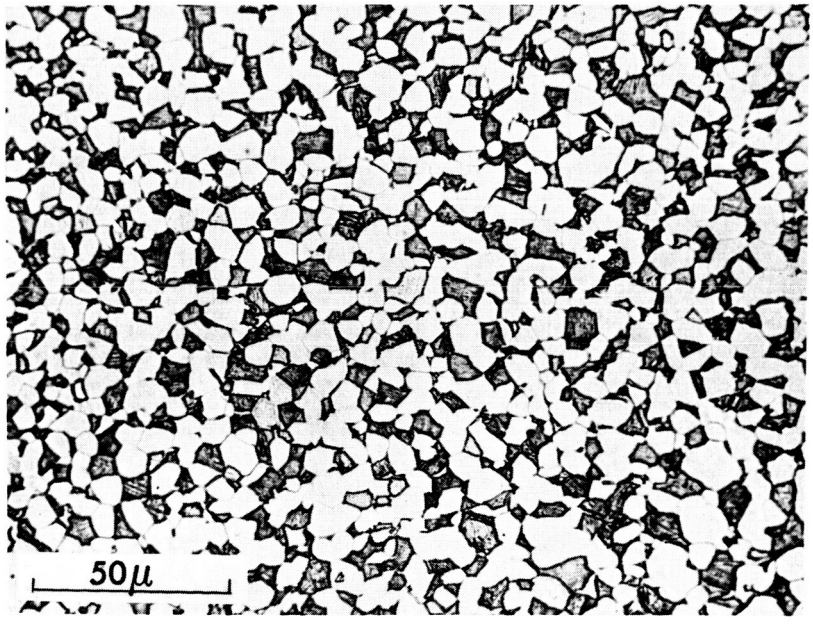

964 500x

Ti 8-1-1 quenched from 1000°C

Fig. 4 Optical Photomicrographs of Quenched Ti:8-1-1 Alloy.

3.3 SCC Under Open Circuit Conditions

Much of the effort this quarter was devoted to studies of stress corrosion cracking in pure solvents or solvents with very low salt concentrations. Precracked specimens were used. With very low salt concentration the resistivity of the solutions is so high that the apex of the crack is essentially electrically isolated from the environment and the potentiostat could not be used. The technique of measuring crack propagation velocities by observing the progress of the crack past pencil lines scribed on the surface was used (Ref. 1). Solvents studied were distilled water, methanol, carbon tetrachloride, methylene chloride and trichlorethylene. SCC occurred in all of these solvents. (SCC did not occur, however, in methanol from one of the bottles of reagent grade material.)

The relative order of velocities in the various solvents at room temperature is indicated in Fig. 5. Velocities were determined by measuring the slope of a crack length versus time curves. Taking a derivative of experimental data increases error by a large factor, and the curves are not exactly linear as will be shown later. Velocity was highest in carbon tetrachloride and increased most rapidly with length of crack in this solvent. Velocities were lower but also increased with length in distilled water and methanol. Velocity appeared to be constant and independent of crack length in methylene chloride. SCC did not occur in trichlorethylene at room temperature but did occur at temperatures above 47°C.

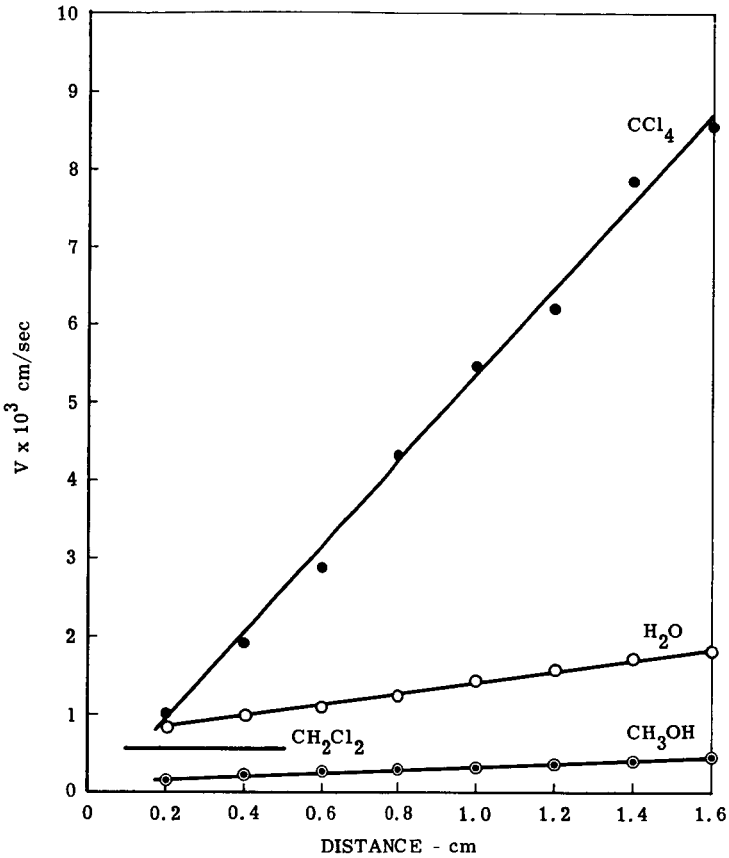

Fig. 5 Velocity of Crack Propagation vs Crack Length in Various Solvents.

Because it was suspected that traces of chloride from some source caused the stress corrosion cracking in distilled water and in methanol, a series of experiments was made to determine the effect of added chloride. (The metal specimens were handled with rubber gloves after washing with acetone and methanol to avoid chloride contamination from hands.) Results are plotted in Fig. 6 as a function of concentration of added sodium chloride. Average slope of the velocity versus crack travel distance from plots like Fig. 5 was used as the most reliable index of the effect of added salt. There appeared to be an increase in crack propagation velocity with chloride concentration in both distilled water and methanol as seen on Fig. 6.

A small amount of silver nitrate was added to distilled water and to methanol in some runs in order to precipitate any chloride contamination present. No visible evidence of a precipitate was observed, but SCC was completely inhibited. To try to resolve the question of whether inhibition was due to precipitation of chloride or to the effect of nitrate ion (Ref. 1) an equivalent molar concentration of potassium nitrate was added in some runs (ppm KNO_3 = =ppm $AgNO_3 \times \frac{101.10}{169.89}$). Potassium nitrate was only slightly less effective, as shown in Fig. 7. A smaller concentration of potassium nitrate, by a factor of about $^1/10$, was required to inhibit SCC in methanol. Sodium sulfate was a similarly effective inhibitor. Sodium fluoride was an inhibitor but a concentration on the order of 1000 ppm was required in distilled water.

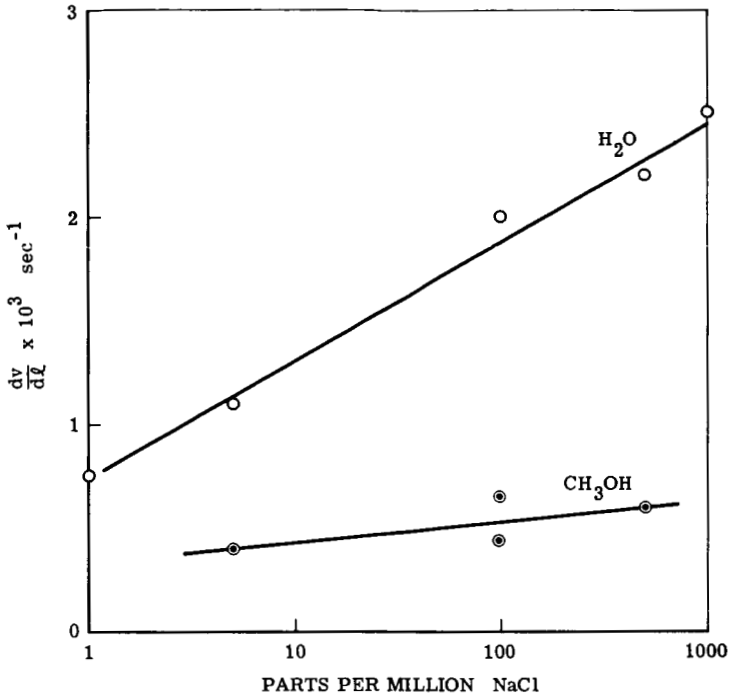

Fig. 6 Effect of Added NaCl on Velocity of Crack Propagation in Distilled Water and Methanol.

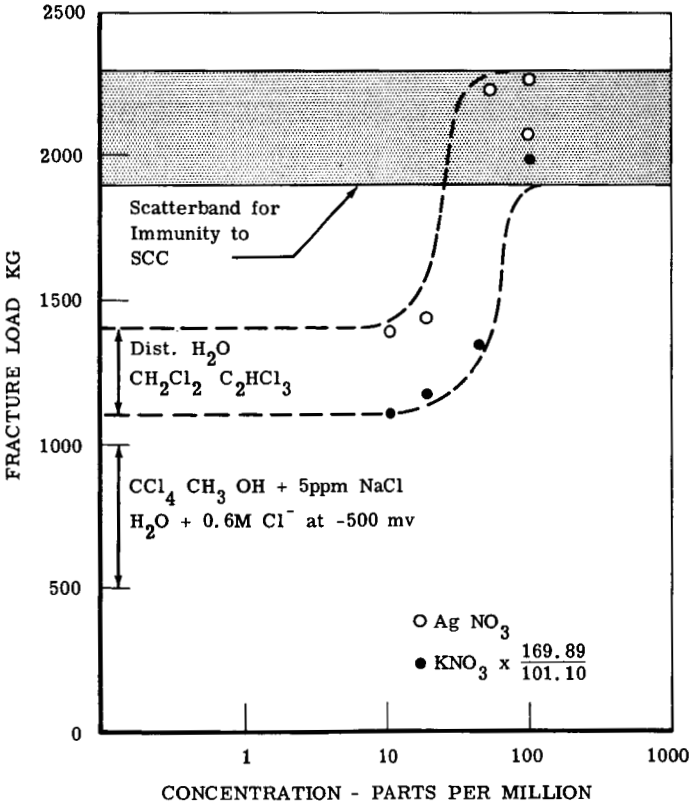

Fig. 7 Effect of Added $AgNO_3$ and KNO_3 on Ultimate Load in Distilled Water.

Considerable effort was spent in finding the best way of correlating the data obtained on crack growth in the various solvents. An analysis of a mass transport - kinetic model for the solvent in the crack suggested a power function

$$(\ell - \ell_o) = K\tau^n \qquad \text{Equation 1}$$

where:

ℓ = crack length in cm at time τ in sec,

ℓ_o = initial crack length , cm,

K and n = constants.

Of the various expressions tried, this proved to give the best correlation for the greatest number of runs.

Typical log-log plots of $(\ell - \ell_o)$ versus τ for the various solvents are shown in Fig. 8. It is to be noted that the slope and therefore the exponent n, is different in the different solvents. With the exception of carbon tetrachloride, a fairly consistent value of n was obtained in each solvent as shown in Table 4. The value of ℓ_o for each run was determined by making a plot of ℓ versus τ^n, using the appropriate value of n for the solvent, and extrapolating to a zero value of τ^n.

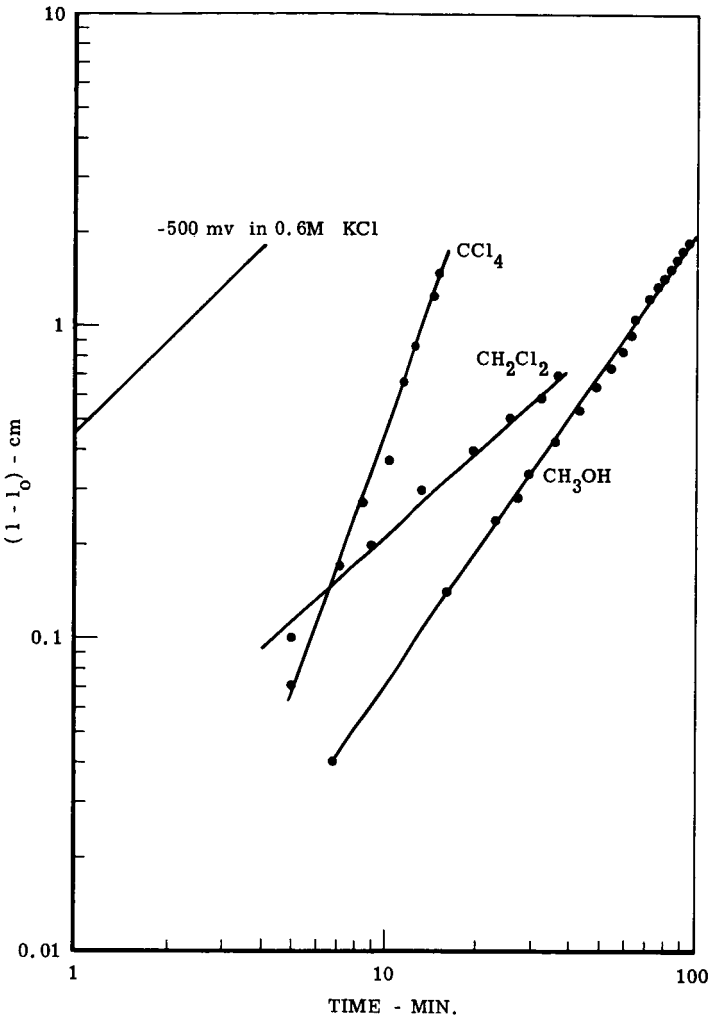

Fig. 8 Relation of Crack Length to Time in Various Solvents.

Table 4 Exponent in Equation 1 for Various Solvents

Run No.	Solvent	Added Salt	Conc. ppm	Temp °C	Ultimate load kg	ℓ_o-cm	n
707	C_2HCl_3	-	-	47	1706	0.04	1.00
708		-	-	68	1376	0.02	1.07
709		-	-	55	1400	0	1.00
710		-	-	77	1268	0.04	1.07
711		-	-	66	1376	0.05	1.07
712		-	-	51	1506	0.04	0.93
713		-	-	60	1362	0.04	0.97
Avg							1.02
734	CH_3OH	NaCl	5	RT	880	0.08	1.46
750		NaCl	500	RT	980	0.08	1.49
751		NaCl	100	RT	940	0.04	1.64
L237		-	-	RT	962	0.03	1.80
L238		NaCl	100	RT	746	0.07	1.47
L239		NaCl	100	RT	980	0.08	1.58
Avg							1.57
737	H_2O	KNO_3	10	RT	1100	-	-
739		-	-	RT	1268	-	-
741		$AgNO_3$	20	RT	1410	0.04	1.55
745		KNO_3	20	RT	1250	-	-
746		KNO_3	50	RT	1350	0.03	1.57
747		NaCl	1	RT	1120	0.01	1.52
748		NaCl	5	RT	1030	-0.04	1.63
764		NaCl	1000	RT	900	0.04	1.51
765		NaCl	100	RT	926	0.01	1.70
768		NaCl	500	RT	956	0.05	1.55
769		-	-	RT	1120	-	-
Avg							1.57
L229	CH_2Cl_2	H_2O	Sat.	RT	1386	0.04	1.25
L231		dry	-	RT	1186	-	-
L234		dry	-	RT	1190	0.04	1.31
L235		H_2O	Sat.	RT	1328	0.04	1.29
Avg							1.28
L230	CCl_4	dry	-	RT	1236	0.10	1.87
L233		dry	-	RT	882	0.15	3.08
L236		H_2O	Sat.	RT	936	0.02	3.58

3.4 Kinetics of Reaction on New Metal Surface

Studies of kinetics of oxidation of newly generated Ti:8-1-1 surface on which multi-layers of oxide are forming have previously been reported (Ref. 1). This work has now been extended to studying kinetics of oxidation and of hydrogen ion reduction on new metal surface during the formation of the first monolayer of oxide. The same cell and 0.060 in. thick, 1/8 in. wide mill annealed notched Ti:8-1-1 specimens described previously (Ref. 1, Fig. 5) were used. A coating of epoxy resin was applied to the specimen to avoid reaction on the pre-existing surface. The resin was scored over the notch in the metal to localize the break in the resin and minimize adhesion failure and exposure of pre-existing titanium surface.

A sudden break was caused by dropping a heavy weight connected through a lever arm to the specimen. Travel of the lever arm was limited so that the new fracture surfaces separated by about 2 mm. Movement of the lever arm closed a microswitch that triggered the sweep in the Tektronix type 545 A oxcilloscope. The camera shutter was open on time exposure during the run.

Runs were made in 0.6 M potassium chloride and concentrated (approx. 12 M) hydrochloric acid. Concentrated HCl was used because it is the electrolyte that is believed to exist near the apex of a propagating crack with a chloride solution as the environment for the metal specimen (Ref. 1). The preliminary data thus far

obtained are rather crude but nevertheless are good enough for order of magnitude estimates of corrosion current density, exchange current density and mixed potential. Further refinements are planned to improve the accuracy of the experiments.

Fig. 9 illustrates typical current-time oscillographs for two different applied potentials. At -800 mv. the initial current pulse was anodic, presumably due to the first oxide layer building up on bare titanium metal. The current then decayed with time. The initial decay is believed to be due to coverage of the surface by oxide. Because a higher overpotential would be required in order to discharge oxide on existing oxide, the current density can be described by

$$i_a = (1 - \theta)\, i_o \exp\left(\frac{\alpha n F \eta}{RT}\right) \qquad \text{Equation 2}$$

for the Tafel condition, where θ is the fraction coverage by oxide. Fraction coverage is related to current density by

$$\frac{d\theta}{d\tau} = \frac{i_a}{Q} \qquad \text{Equation 3}$$

where Q is the coulombic charge equivalent to a monolayer of oxide ($Q \approx 425 \times 10^{-6}$ coulomb/cm^2, Ref. 1). Extrapolation of the limiting slope at time zero to zero current (Fig. 9) gives the time to form a monolayer at a constant current equal to the initial value. The initial current density for oxide formation based on Equation 3

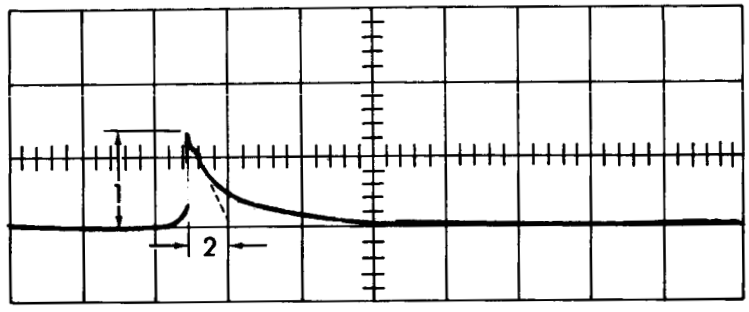

Conc. HCl at -800 mv (Net Anodic Current)

Vert. 0.1/cm (across 10Ω),
Horiz. 2 ms/cm

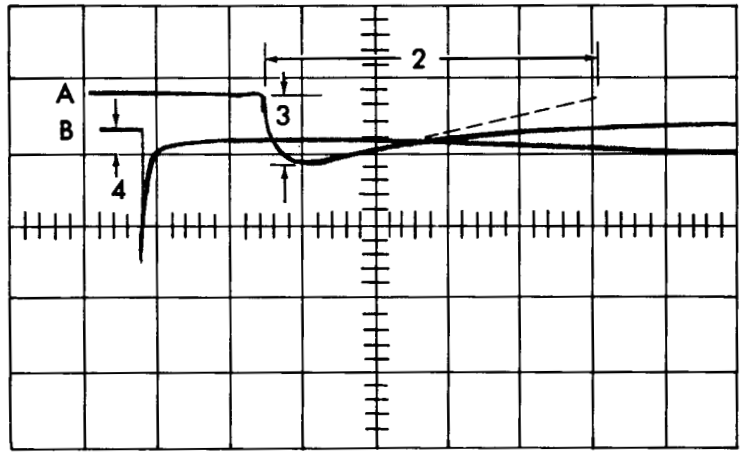

Conc. HCl at -960 mv (Net Cathodic Current)

(A) Vert. 0.1 v/cm (across 10Ω),
Horiz. 2 ms/cm
(B) Vert. 0.05 v/cm (across 10Ω),
Horiz. 0.2 sec/cm

Fig. 9 Current - Time oscillographs (1 Initial Oxidation peak on bare Ti, 2 Time to form oxide monolayer at initial oxidation current density, 3 Initial H^+ reduction peak on bare Ti, 4 H^+ reduction on TiO_2)

is therefore

$$i_a = \frac{Q}{\tau_o} \qquad \text{Equation 4}$$

At a potential of -910 mv. the initial current was cathodic due to hydrogen ion discharge. The current subsequently decayed and presumably this was due to oxide coverage by simultaneous oxidation. By determining τ_o as above, the true oxidation current density can be estimated by potentials where the net measured current is cathodic. The net current density is

$$i = i_a - i_c \qquad \text{Equation 5}$$

where the subscripts a and c refer to anodic and cathodic respectively. The measured net current is therefore not the actual anodic or cathodic current, but a somewhat smaller value depending on how far displaced from the mixed potential or corrosion potential, where $i = i_a - i_c = 0$.

An estimate of current for discharge of hydrogen ion on TiO_2 was also made as shown in Fig. 9. A slow trace was used to obtain this value.

The anodic and cathodic current densities as a function of potential are summarized in Fig. 10. A new area of 0.05 cm^2 was used to calculate current densities from the peak currents and hydrogen ion discharge on TiO_2. Equation 4 gives the true anodic

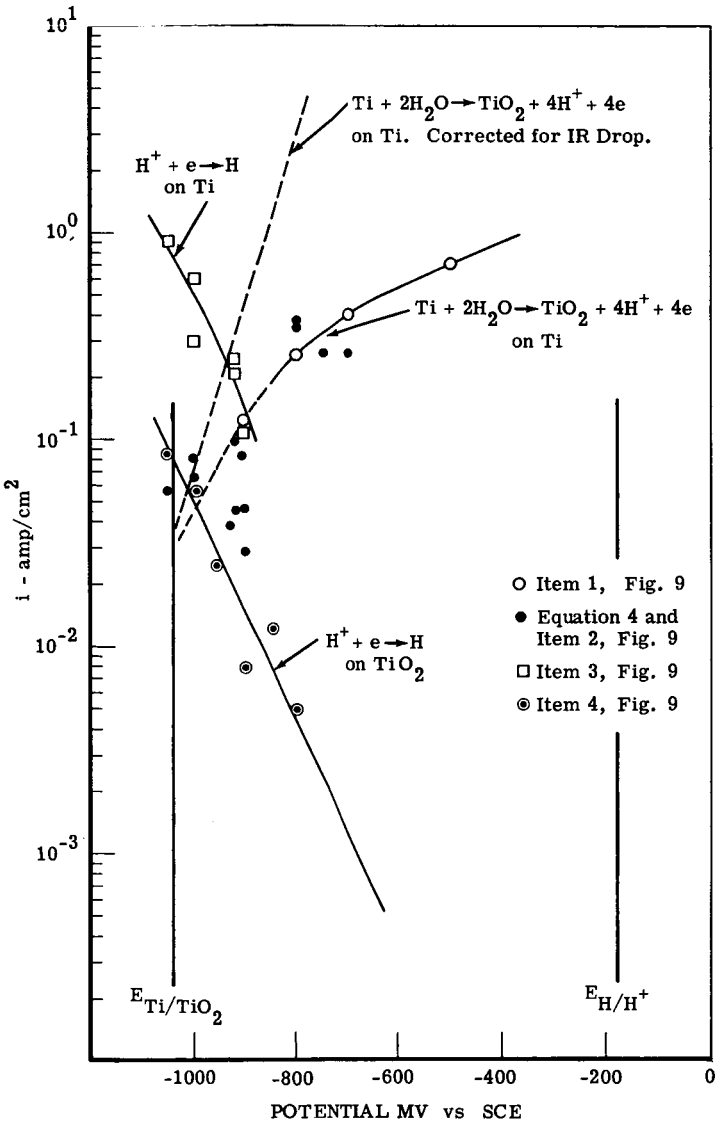

Fig. 10 Summary of Kinetic Data for New Ti:8-1-1 Surface in 12 M HCl.

current density. Considering the scatter of the data and all of the assumptions made, there is a reasonably good correspondence between net anodic current density from the peaks and true anodic current density from τ_o and Equation 4. At high current densities there is a relatively large IR drop between the Luggin capillary tip on the two new surfaces. This potential drop may be estimated by

$$\Delta\phi = \frac{i}{K} \; x\Delta \qquad \text{Equation 6}$$

At a current density of 1 amp/cm^2, a Luggin capillary to electrode spacing of 0.3 cm and a conductivity of 0.5 Ω^{-1}cm^{-1} for 12 M HCl (Ref. 5), the potential drop is 0.6 volts. An anodic Tafel line of 120 mv per decade slope is drawn using this IR correction.

Probably the most significant conclusion to be drawn from these data is that the corrosion potential of newly exposed Ti:8-1-1 surface in 12 M HCl appears to be about -900 mv. If the electrolyte within a propagating crack in a chloride environment is concentrated HCl as predicted (Ref. 1), then this would explain the -900 mv intercept in the crack propagation velocity vs potential plot (Ref. 1).

A second bit of information useful in the analysis of SCC is that hydrogen ion is reduced and the current density is on the order of 10^{-1} to 1 amp/cm^2 taking the IR correction into consideration. This will be discussed further in the next section.

The results in 0.6 M KCl were similar except that the IR error was about an order of magnitude larger and the corrosion potential shifted to -1750 mv. This 850 mv shift is twice the value expected for the change in PH. Further work is needed to resolve this difference.

3.5 Theory

Previously (Ref. 1) it was shown that the oxide wedging mechanism is not probable at the crack propagation velocities exhibited by Ti:8-1-1 alloy. The new kinetic data substantiate the earlier calculations. The time to form a monolayer of oxide at constant current is

$$\tau_m = \frac{Q}{i_a} \qquad \text{Equation 7}$$

Assuming $i_a = 10^{-1}$ to 1 amp/cm^2 gives $\tau_m = 4.25 \times 10^{-3}$ to 4.25×10^{-4} seconds for monolayer oxygen coverage. For a crack propagation velocity of 10^{-2} cm/sec, the distance to obtain the first monolayer would therefore be 4.25×10^{-5} to 4.25×10^{-6} cm. But the current density decays with θ, which gives a longer time and distance. Combining Equations 2 and 3 and integrating gives

$$\tau_m = \frac{Q}{i_{a_{initial}}} \ln \left(\frac{1}{1-\theta}\right) \qquad \text{Equation 8}$$

If it is assumed that 99% coverage is required before the second layer starts building, Equation 8 gives $\tau_m = 2 \times 10^{-2}$ to 2×10^{-3} sec. and corresponding distances of 2×10^{-4} to 2×10^{-5} cm for the first monolayer to be essentially complete. The argument that growth of a monolayer within this distance (Ref. 1, Fig. 32) should not cause a wedging force therefore still stands.

Previously it was not possible to pass judgment on the possible hydride mechanism of cracking. The new kinetic data provide a basis for examining the feasibility of this mechanism. The tentative conclusion at this time is that the hydride mechanism is not likely as the cause of SCC in the Ti:8-1-1 alloy experiments.

The argument is similar to that used for oxide. In the apex zone with less than a monolayer of oxide the metal would appear to be at the mixed potential and the anodic and cathodic current densities would be equal. Assuming one hydrogen per titanium on the surface gives $Q_H = 212 \times 10^{-6}$ coul/cm^2. Assuming also that current density decreases with θ by Equation 2, gives a distance of 10^{-4} to 10^{-5} cm for 99% doverage of a monolayer (ignoring the simultaneous coverage of oxide). Unless the hydrogen atoms have an unusually high surface mobility the concentration of hydrogen atoms at the apex would be too small to produce significant hydride.

It is likely that hydrogen atoms would diffuse into the metal as fast as they are formed, rather than sit on the surfaces as an adsorbed layer. It is instructive to consider the limiting case of complete diffusion into the metal of all of the discharged hydrogen. In order to use a simplified model for which results can be readily calculated, consider that the metal is divided into thin sheets conductive to hydrogen separated by infinitesimally thin non-conducting membranes. The sheets, Δy in thickness, are normal to the planes of the new surface and parallel to the crack front. Unsteady-state diffusion at a constant surface flux occurs (ignoring change due to θ)

at the edge of each of these sheets, starting at time of formation of the cut edge. The age of the cut edge is

$$\tau_y = y/V \qquad \text{Equation 9}$$

The concentration of hydrogen at the surface, y distance from the geometric apex for a constant surface flux, by analogy to heat transfer is (Ref. 6),

$$c_{x=0} = 1.13 \frac{j_{x=0}}{D_H} \sqrt{D_H \tau_y} \qquad \text{Equation 10}$$

where x is the distance into the sheets from the edge. Assuming the upper limit for current density of 1 amp/cm^2,

$$j_{x=0} = \frac{i}{ZF} \approx \frac{1}{10^5} = 10^{-5} \text{ mole/cm}^2\text{sec.}$$

The diffusivity of hydrogen in titanium is not known, but a value recently determined for hydrogen in iron of about 10^{-5} cm^2/sec (Ref. 7), will be used. The age of the new surface is zero at the apex, but a distance of atomic dimensions will be used for illustration. Assuming y = 2 x 10^{-8} cm and V = 10^{-2} cm/sec, gives τ_y = 2 x 10^{-6} sec. Putting these values in Equation 10 gives $c_{x=0} \approx 3 \times 10^{-6}$ mole/cm^3. Converting to mole fraction of hydrogen in titanium gives $N_H = \frac{3 \times 10^{-6}}{4.5/47} \approx 3 \times 10^{-5}$. The hydride mechanism appears highly unlikely under the conditions of our experiments if this analysis is correct.

A further argument against the hydrogen mechanism is that SCC occurs in carbon tetrachloride at relatively high velocity. It made little difference in the velocity whether the carbon tetrachloride was saturated with water or dried over Drierite. Because carbon tetrachloride has no hydrogen in it and water was reduced to a very low level, a hydride mechanism appears extremely unlikely in this solvent. Further, adding benzene, a hydrocarbon, had the effect of decreasing crack propagation velocity.

If chloride, bromide and iodide are the only SCC agents, as previously found (Ref. 1), the question arises as to the source of these in the methanol and distilled water experiments. Chloride ion is a common contaminant in all materials and it is conceivable that a "super purification" of methanol and distilled water plus conducting the SCC experiments in a clean room would be required to eliminate exterior contamination. Mr. F. Drosden of Boeing, Huntsville (Ref. 8), however, suggested that the metal itself may be a source of chloride because it is made by reduction of titanium tetrachloride. A subsequent call to Titanium Metals Corp. (Ref. 9) revealed that the chloride level of commercial titanium metal is on the order of 10 to 20 parts per million. This level would be high enough to give a significant concentration of chloride to the electrolyte in the wedge shaped crack by leaching chloride from the walls. This lead is being pursued. Analyses for chloride in the metal specimens used are underway and vacuum heat treating to remove chloride is being investigated.

A mathematical model including concentration of chloride from the crack walls in the solution predicted the power law (Equation 1) that best fit the data. The development is not in its finished form so presentation of it will be deferred to the next quarterly report. This analysis is an extension of work begun prior to the contract in collaboration with Prof. E. A. Grens of Berkeley on an analysis of current distribution in a propagating crack. Results of the study will be presented at the 1967 spring Electrochemical Society Meeting in Dallas. The extended abstract for the paper is included in Appendix A.

4.0 CONCLUSIONS

The following conclusions are based on the work accomplished in the period of October 1 through December 31, 1966.

1. Precracking the notched duplex annealed Ti:8-1-1 tensile specimens resulted in lower ultimate loads under SCC conditions. Precracking mill annealed specimens resulted in a sensitivity to SCC not previously observed.

2. Two more anions, cyanide and thiocyanate did not appear to produce SCC in Ti:8-1-1. To date the only anions found to produce SCC in Ti:8-1-1 are chloride, bromide and iodide.

3. The ultimate strength of precracked Ti:8-1-1 specimens is very sensitive to heat treatment when tested at -500 mv in 0.6 M KCl. This effect is believed to be related to grain size and mean free path within the α-phase, α - β phase differential composition effects and possible changes in short range order.

4. Ti:8-1-1 was found to be susceptible to SCC in the following pure solvents: distilled water, methanol, carbon tetrachloride, methylene chloride, and trichlorethylene. There is a wide variation in crack propagation velocities between solvents. Crack length could be related to time by the relation $(\ell - \ell_o) = K \tau^n$, where n is relatively constant for each solvent (except for CCl_4) but varied between solvents.

5. SCC could be completely suppressed in distilled water and in methanol by addition of nitrate or sulfate at concentrations on the order of 10 - 100 ppm. Addition of chloride to the solvents increased SCC susceptibility and crack propagation velocity.

6. Electrochemical kinetics experiments on newly generated Ti:8-1-1 surface in concentrated HCl indicate that the corrosion potential is about -900 mv versus SCE in this medium. This is consistent with the -900 mv intercept on the velocity versus potential relation for SCC in chloride solutions, as concentrated HCl is predicted at the apex of the SCC crack under these conditions.

7. The kinetics experiments indicate that hydrogen ion is reduced in the apex zone of a propagating stress corrosion crack but that the rate of hydrogen formation is too small to form a significant amount of hydride. The hydride mechanism of SCC in Ti:8-1-1 therefore appears unlikely.

8. Chloride leached out of the metal is suspected as the SCC agent in distilled water and methanol environments.

5.0 FUTURE WORK

The following items of work are planned for the immediate future:

1. Test titanium-aluminum alloys in the range of 8% to 10% aluminum in order to correlate SCC results with simple and known metallurgy. (Delivery of alloy sheets is imminent.)

2. Determine relationship of SCC velocity to heat treatment and metal structure.

3. Obtain chloride analyses for titanium metal. Prepare specimens with different chloride levels and determine effect on velocity in distilled water and methanol environments.

4. Refine and extend kinetic studies to obtain exchange current densities, Tafel slopes and other electrochemical parameters needed for analysis of crack propagation velocity.

5. Refine and extend mass transport-kinetic model to apply to conditions near the apex of a propagating stress corrosion crack.

6. Relate the electrochemical model to the pertinent metallurgical parameters.

PRECEDING PAGE BLANK NOT FILMED.

6.0 REFERENCES

1. T. R. Beck, Boeing Document, D1-82-0554, July, 1966.

2. T. R. Beck, Contract NAS 7-489, Quarterly Progress Report No. 1, October, 1966.

3. M. J. Blackburn, Trans. ASM, 59, 876 (1966).

4. M. J. Blackburn, Trans. ASM, 59, 862 (1966).

5. International Critical Tables.

6. H. S. Carslaw and J. C. Jaeger, "Conduction of Heat in Solids", Oxford Press, 1959.

7. W. Beck, J. O"M. Bockris, J. McBreen and L. Nanis, Proceedings of the Royal Society, A, 290, 220 (1966).

8. Telephone conversation, F. Drosden, Boeing, Huntsville, Ala. to T. R. Beck, November 16, 1966.

9. Telephone conversation, T. R. Beck to E. Millaway, Titanium Metals Corp., Henderson, Nev. week of November 21, 1966.

PRECEDING PAGE BLANK NOT FILMED.

7.0 APPENDIX

Extended abstract sent to the Electrochemical Society for May, 1967, meeting in Dallas.

PRECEDING PAGE BLANK NOT FILMED.

ANALYSIS OF CURRENT DENSITY DISTRIBUTION IN A PROPAGATING STRESS CORROSION CRACK

T. R. Beck* and E. A. Grens II**

*Boeing Scientific Research Laboratories
P. O. Box 3981, Seattle, Wash. 98124

** Department of Chemical Engineering
University of California
Berkeley, Calif. 94720

The purpose of this work was to develop a quantitative model for the kinetic and mass transport processes in a propagating stress corrosion crack. The predictions of the model have been compared to experimental stress corrosion cracking data for a titanium alloy reported previously (1).

The model for the one-dimensional treatment is given in Fig. 1. A crack in a metal sheet of unit thickness is assumed to have a wedge shape with a small constant included angle γ, expressed in radians. The crack propagates at a constant velocity V. The electrolyte, which is assumed to completely fill the crack, is considered stagnant (no convection) with respect to the apex of the crack. All fluxes in the electrolyte are therefore taken as relative to a coordinate system moving with the apex. A portion of the crack depth, extending a distance ℓ from the apex is examined. Beyond this distance there is significant flow of current and electrolyte from the faces of the metal sheet (sides of the crack) and the electrolyte can be assumed to be well mixed at conditions $\phi = \phi^o$ and $C = C^o$ (mouth of crack). The region under consideration is divided into three zones: one of length δ_o, of molecular dimensions at the apex; a zone $\delta - \delta_o$ with less than a monolayer of oxide; and a zone $\ell - \delta$ with more than a monolayer of oxide.

The electrochemical reactions chosen for the analysis are:

$$Ti + 4X^- \rightarrow TiX_4 + 4e \qquad \text{Reaction 1}$$

$$Ti + 2H_2O \rightarrow TiO_2 + 4H^+ + 4e \qquad \text{Reaction 2}$$

$$4H^+ + 4e \rightarrow 4H \qquad \text{Reaction 3}$$

Reaction 1, with a halide ion X^-, is considered to occur at the apex and to be responsible for the stress corrosion cracking. It may also occur under some conditions in the zone with less than a monolayer of oxide. Reaction 2 occurs over the whole length of the crack. Reaction 3 may occur in the acid zone near the apex with the hydrogen dissolving in the metal.

The current density (reaction rate) at the crack surface is determined by electrochemical kinetics and by high-field conduction through the oxide layer. The kinetic expression used is the Tafel approximation

$$j_s = i_o \exp \frac{\alpha n F}{RT} (\phi - \phi_e) \tag{1}$$

and the high field conduction equation,

$$j_s = j_o \exp \frac{B\Delta\phi}{t} \tag{2}$$

using the usual symbol convention. Appropriate correction must be made for oxide coverage θ in the zone, $\delta - \delta_o$.

Three ions are assumed to carry the current in the electrolyte: the cation and anion of the dissolved salt from the bulk solution and the hydrogen ion generated by reaction 2. The fluxes of the three ions along the axis of the crack are:

$$N_+ = -D_+ \frac{dC_+}{dy} - z_+ D_+ C_+ \frac{d\Phi}{dy} \tag{3}$$

$$N_- = -D_- \frac{dC_-}{dy} - z_- D_- C_- \frac{d\Phi}{dy} \tag{4}$$

$$N_H = -D_H \frac{dC_H}{dy} - z_H D_H C_H \frac{d\Phi}{dy} \tag{5}$$

where $\Phi = \frac{F}{RT} (\phi - \phi^{apex})$.

The condition of electroneutrality gives:

$$z_+ C_+ + z_- C_- + z_H C_H = 0 \tag{6}$$

The flux of the metal ion, N_+, is zero because this ion does not participate in the electrochemical reactions. If reaction 1 occurs only at the apex and if the surface chloride formed is subsequently displaced by oxide, the anion flux, N_-, is also zero through most of the crack. The current density at any point is

$$i = F \sum z_i N_i \tag{7}$$

The total current in the electrolyte at point y for a sheet of unit thickness is:

$$I = i\gamma y \tag{8}$$

for a small angle crack, where i is the current density in direction y. By conservation of charge at quasi-steady state:

$$dI = \gamma(i dy + y di) = 2 j_s \, dy \tag{9}$$

For N_+ and N_- both effectively zero, the preceeding equations can be rearranged to give:

$$\frac{di}{dy} = \frac{1}{y}\left(\frac{2j_s}{\gamma} - i\right) \tag{10}$$

$$\frac{d\Phi}{dy} = -\frac{i}{FD_H C_-^o \left\{ z_+(z_+-1)e^{z_+(\Phi^\circ-\Phi)} + z_-(z_--1)e^{z_-(\Phi^\circ-\Phi)} \right\}} \tag{11}$$

$$j_s = j_o \exp\left\{ \frac{BVRT}{F} \cdot \frac{\Phi-\Phi_e-\Phi_f-\Phi_x}{k\int_{\delta_o}^{y} j_s dy} \right\} \qquad \text{at } y \geq \delta$$

$$= i_m(1-\theta)\exp\{\tfrac{n}{2}(\Phi-\Phi_e)\} + i_o\theta \qquad \text{at } y \leq \delta \tag{12}$$

where: Φ_e = Reversible potential

Φ_f = Flade potential

Φ_x = overpotential for oxide deposition on oxide

θ = fractional oxide coverage on surface = $k\int_{\delta_o}^{y} j_s dy$

i_m, i_o = exchange currents on metal/oxide for reaction 2

k = proportionality between deposition and film thickness

Φ° = Φ at $y = \ell$

Equations (10) (11) and (12), together with the boundary conditions:

at $y = \delta_o$: $\Phi = 0$ $\qquad i = i^{apex}$

at $y = \delta$: $\theta = 1$

are solved by a Runge-Kutta-Gill numerical integration procedure, starting with an assumed value of Φ° (Φ at $y = \ell$), integrating from $y = \delta_o$ to $y = \ell$ to find a revised Φ°, and iterating this process to convergence. The calculations are implemented by a digital computer and converge in a reasonable number of iterations.

Results are presented in the form of current density versus y at given values of $\Phi°$ and current and velocity versus $\Phi°$. The calculations are compared to experimental data for stress corrosion cracking of Ti:8%Al-1%Mo-1%V alloy.

References

1. T. R. Beck, "Stress Corrosion Cracking of Titanium Alloys," Presented at ECS 130th meeting, October 10, 1966 (submitted to Journal of ECS).

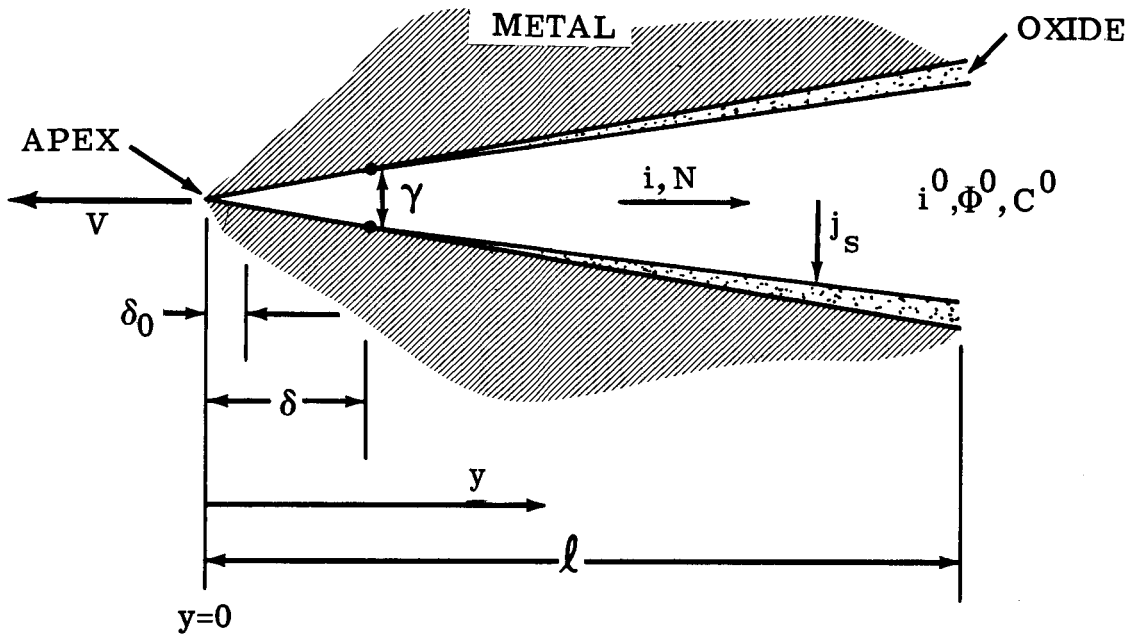
METAL
OXIDE
APEX
V
γ
i, N
i^0, Φ^0, C^0
j_s
δ_0
δ
y
ℓ
y=0